2 Physics and Technology of Fusion

Work in fusion plasma physics and technology includes 13 tasks. The tasks are grouped under the six following sub-headings corresponding to the EFDA Task Forces and Topical Groups:

- Integrated tokamak modelling
 - Tokamak modelling
 - Nonlinear dynamics of fast ion driven plasma modes near instability threshold theoretical basis for integrated tokamak modeling
 - Stochastic processes and stochastic representations for the kinetic equations of a gas of charged particles

Plasma-wall interaction

- Portable LIBS device for calibrated measurements of material deposition and composition of the walls on plasma source
- Study of laser based diagnostic methods, photonic cleaning and spectroscopy (including LIBS) in perspective of next-step fusion devices (including ITER)
- Laser-induced removal of fuel and co-deposits from plasma facing components in tokamaks. Characterisation of gas, plasma and dust released from laser-irradiated samples and investigation of laser-irradiated surface of samples Including:

Removal of the deposited materials by laser ablation techniques. Investigation of carbon layers with varying concentrations of Al (Be analogue), W and W-Be

Investigation of film break-up processes during laser cleaning. Monitoring of the composition of gases and particles released from the target

Irradiation of TEXTOR and AUG samples containing material mix of carbon and tungsten by the Nd:YAG pulsed repetitive laser. Use of optical spectroscopy together with ion diagnostics to characterize chemical composition of samples

- Studies of material erosion and re-deposition on plasma facing components from the present day machines. Characterization of exposed PFCs with various microscopic and analytical techniques (TEXTOR and AUG) (High-Z materials)
- Development of material science and advanced materials for DEMO
 - Ab-initio study of defects configurations and their interactions in W-Ta and W-V model alloys
 - Development of W-EUROFER based on PPS and a transition layer incorporated between both materials to decrease thermal stresses
 - O Hydrostatic Extrusion (HE) processing of ODS ferritic steel: microstructure characterisation, mechanical properties and thermal stability
- Fusion plasma diagnostics
 - Activation technique in a cross-check experiment for high resolution neutron spectrometry
 - o Diamond and track detectors to detect escaping fast alpha particles
 - o Cherenkov detectors for fast electron measurements: new diagnostics for Tore-Supra

Physics and Technology of Fusion

- o High-temperature Hall sensor for future applications in measurements of magnetic field in fusion reactors
- o Microwave diagnostic development for JET
- Inertial fusion energy "keep-in-touch" activity
 - Coordinated study of phenomena related to impact fast ignition of ICF targets.
 Investigation of properties of the plasma jet generated from of materials with various atomic number for ICF applications
- Socio-Economic Research
 - o Awareness of Fusion Energy: Action-research in fusion awareness and in communication capacity building among selected stakeholders

Physics and Technology of Fusion
Integrated Tokamak Modelling

Tokamak modelling

The activity in the frame of ITM project was focused on developing the testing procedure of European Transport Solver (ETS) and delivering the impurity transport module (ITS).

It was assumed that ETS would solve the 1D time evolution equations for poloidal flux, the densities, temperatures and toroidal velocities for all ions. The ETS contains several numerical procedures (solvers) to solve the single equations. The iteration is applied to take into account the coupling between the equations. The choice of numerical procedure is defined by code parameter. The method of manufactured solution was used to calculate the source terms of the equations from the assumed profiles for the solution, transport coefficient and metric coefficients. The calculated source terms, transport coefficients and metric coefficients can be used in ETS to find the numerical solutions and compare with analytical profiles. The main advantage of using this procedure is the possibility to compare the solution of the system of nonlinear-coupled equation with the exact one. The manufactured solution method was implemented in the module Analytics with the input and output in the form of the CPO's (consistent physical object) and in this form can be transformed into actors in the frame of data processing system Kepler. In the module Analytics the arbitrary number of ion can be analyzed and all assumed in ETS boundary condition can be used. The non-linear coupling due to energy and momentum exchange terms was also included. The robustness of the numerical scheme used in ETS for different types of the data and its smoothness can be check. The several sets of analytical solution have been prepared with different temperature profiles corresponding to typical profiles of JET, ITER and Demo reactors. Special script has been prepared to perform the test of the scheme for all prepared set of analytical profiles. The results are written in the special data base. The special programme in python has been developed for graphical presentation of the results.

The behavior of the solvers in case of the strong dependence of the transport coefficients on the derivative of the solution has been tested. In order to simplify the analysis the single diffusion equation in cylindrical geometry has been used. It was assumed that the diffusion coefficient undergoes the rapid drop when the e-folding length becomes lower the given critical value of the e-folding length.

$$\begin{split} \frac{\partial \rho n}{\partial t} - \frac{\partial}{\partial \rho} \rho D \frac{\partial n}{\partial \rho} &= \rho Q \quad where \quad \rho \in [0,1] \\ D &= D_1 \quad for \quad \frac{-n}{\partial n/\partial \rho} < L_{cr} \quad ; D = D_2 << D_1 \quad for \quad \frac{-n}{\partial n/\partial \rho} > L_{cr} \; . \end{split}$$

For this model of the diffusion the stationary solution has many solutions defined by the position of the discontinuity of the diffusion coefficients. The manufactured method was extended to this case. The profile of the flux function (continuous function) was assumed and the source term is calculated. The equation is solved numerically and the results compared with the assumed profile of the solution. The tested solvers can reproduce the analytical solutions for stationary case. However, in case of time evolution the position of the transport barrier is given with significant error. We have also performed a calculation showing an example of the possibility of passing from L mode (lower confinement) to H mode (higher confinement). The calculation has been performed for D1=1, D2=0.5, Lcr=0.8 and the source term of the form $Q=s(1-\rho)$. The calculation consists of three stages. At first we start with the initial condition n=0 and the calculations are performed with s=6 until a steady state is reached. For this steady state there is no jump in the derivative. Then, at a second stage, the value of s is increased to 8 and the calculation is performed until another steady state is reached. At last the value of s is reduced to 6 and another steady state is obtained. The steady states at the end of the second and third stages have a jump in the derivative at the same value of ρ (Fig. 1). Two solvers implemented into ETS have been used. Solver2 is based central finite difference approximation in space and forward Euler formula in time. Solver7 corresponds to implementation of the method used in code RITM.

Moreover, the final solution corresponds to a higher confinement than the one obtained at the first stage, because the confinement depends on the position of the derivative discontinuity. The steady solutions obtained with both solvers gives the function corresponding to analytical steady solutions. Unfortunately,

the difference of the critical points ρ_{cr} obtained by the two solvers at the final stage shows that the confinement is probably calculated with a significant error. At this point it cannot be decided which solver gives more accurate results in this context. The problem should be considered in the future and the analyses should be extended to the continuous analytical model of the transport.

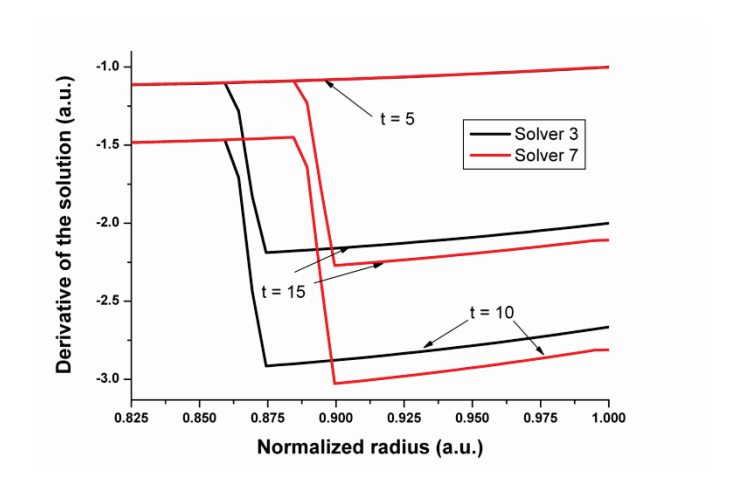


Fig. 3. Derivatives of the steady state solutions obtained with solvers 3 and 7 at the end of the three consecutive stages

The impurity transport solver solves the 1.5D transport equations for the density of each ionization state for each impurity. Different ionization states are coupled by the ionization and recombination processes. The equations are solved successively for each ionization stage of impurity. The time interval is split into two subintervals. In the first half step the equation are solved starting from the lowest ionization stage to the highest ionization stage. In the second half step, the 1D equation is solved starting form the highest ionization stage to the lowest one. In the solution of each ionization stage the new value of impurity density calculated in previous ionization stage is used. In order to estimate the error the manufactured solution method has been used. The manufactured solution methods has been used to testing the accuracy of ITS. The impurity transport solver has been included into ETS workflow. The example of the test of the accuracy for solver3 of method is presented in Fig.2 for neon.

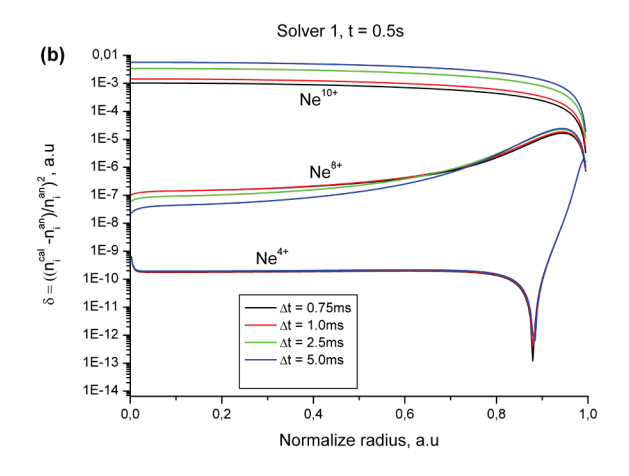


Fig. 2. The influence of the time steep on the relative error of the numerical solution for solver 3 for the time: t = 0.5s

The numerical analysis of the line radiation losses in DEMO B and DEMO C has been performed using the code COREDIV, previously used to model the regimes of ITER reactor for carbon, nickel and

molybdenum as sputtered impurity. In the presented analysis the tungsten as sputtered impurity and argon as seeded impurity is considered. The sputtering of tungsten includes contributions from all ions interacting with divertor plates. The code COREDIV solves in self-inconsistent way the core and boundary region. The core part of the model is based on a standard set of equation describing multifluid radial transport. The transport equations for densities of bulk ions and of impurity ions for each ionization state are solved. It is assumed that all ions have the same temperature. In the equations for ion and electron temperature the energy sources: alpha heating and Ohm heating are calculated according to plasma profiles, whereas for the auxiliary heating the parabolic-like deposition profile is assumed. The energy losses are defined by bremsstrahlung, synchrotron and line radiation. The anomalous heat conductivity is given by simple model with multiplication constant fitted to get the agreement of confinement time with ELMy H-mode scaling law. The core and SOL transport equations are solved simultaneously. This requires that the core and edge part of COREDIV be iterated alternatively until the steady state solution is reached. Since the procedure is time consuming the simple model of SOL has been chosen. In the SOL the 2D EPIT code is used. The code EPIT is based on Braginskij like equation for bulk plasma and rate equation for each ionization state of each impurity. The continuity equation, the parallel momentum conservation equations for every ion species and the equations for electron and ions energies are solved. The hydrogen recycling coefficient is an external parameter. We assumed that seeded impurities are introduced by gas puff located closed to the midplane and their recycling at the target plates is described by the recycling coefficient R = 0.925. The scan with respect of Ar source intensity has been performed. The obtained results show that the power load to the plate can be reduced but an increase of the impurity concentration leads to a decrease of alpha heating showing that the procedure cannot be applied successfully. However, present simulation has been performed using the very simplified model of the transport. A more refined physical model should be used to verify the above conclusion.

Nonlinear dynamics of fast ion driven plasma modes near instability threshold – theoretical basis for integrated tokamak modelling

In 2009, we have continued the research program of examination of physical content of Berk and Breizman (BB) model. The model describes nonlinear dynamics of plasma modes resonantly interacting with fast ions near instabilities threshold. The model possesses some kind of universality and in some extent can be applicable to Alfven modes in tokamak. Our group has conducted investigations in two specific directions. The first one was devoted to the better understanding of the totality of the phenomena described by (BB) model, in particular the physical nature of instability which appears for small values of the collision frequency v. Second direction of research concerned the extension of the existing model to a multimode case. In the course of investigations we have noticed that the original BB theory, which involves integro-differential equation, may be replaced by an ordinary differential equation of fifth order. After further simplifications we have obtained a relatively simple description of the dynamics of plasma modes in the form of nonlinear oscillator equation. As a result our simplified model, which deals with ordinary differential equations reduces the time of numerical calculations from hours to seconds. This model not only enables the faster numerical modelling of complicated plasma wave–fast ions interaction but also contains essential physics and some universality of the BB model. Moreover, it can be easily extended to describe the evolution of greater number of the plasma modes. This fact causes that our simplified model after further modifications can be interesting for EFDA-ITM applications in the scope of Alfvén Modes electrodynamics.

Unfortunately, at the present stage, what was mentioned before, the numerical solutions of both simplified and BB model equations contain some critical parameters below which the models become unstable and the physical nature of such instability is still unexplained. As a result the development of a code for the EFDA Task: WP10-ITM-IMP5: (Code development for global stability analyses of Alfvén Modes in realistic tokamak geometries and in the presence of nonperturbative fast ion excitations) with a special attention to global stability analysis specifically, needs much more time.

Stochastic processes and stochastic representations for the kinetic equations of a gas of charged particles

The random processes of diffusion in \mathbb{R}^n and jumps on a fractal $\Gamma \subset \mathbb{R}^n$ have been studied in terms of the Dirichlet forms E. The jump measure J of the Dirichlet form is defined as an image of a jump measure j of a process in a non-Archimedean metric space. As the result the jump intensity depends on the hierarchical structure of Γ rather then the geometric distance in \mathbb{R}^n . For a class of fractals in \mathbb{R}^2 we find a condition on the measure j so that the Dirichlet form E is regular. The condition is given in terms of Hausdorff dimension of Γ . These results are presented in the paper: W. Karwowski, K. Yasuda Dirichlet Forms for Diffusion with Jumps on Fractals. The regularity problem. (to be published) There are strong indications that if E is not regular then the process after a limited time is trapped in Γ and thus reduced to a pure jump process. This conjecture is presently examined. When it is confirmed the above results describe the mathematical mechanism of the passing from "diffusion+jumps" to "pure diffusion" phase.

Physics and Technology of Fusion
, 0.00 0 0 0.00 0 0.00
Plasma-wall interaction

Portable LIBS device for calibrated measurements of material deposition and composition of the walls on plasma source

The aim of the task was to perform LIBS (Laser Induced Breakdown Spectroscopy) tests on the calibrated samples provided by the NILPRP in the framework of the task. The samples were produced by magnetron sputtering and they contained material mix relevant to the one foreseen for components of the next step tokamak. In particular, two sets of samples have been investigated:

- Titanium substrates with 10 μm tungsten layer with 1-2 μm Molybdenum interlayer. Carbon and oxygen as surface contamination.
- Titanium with C:W layers of two fixed ratios contaminated with O on the surface.

The experiments with the use of the Mechelle 5000 spectrometer (fig.1) equipped with ICCD iStar camera of the laser plasma generated by 3-3.5 ns, 300 mJ pulses of Nd:YAG (1064 nm wavelength) with repetition rate up to 10 Hz allowed for reliable qualitative analysis of all samples and for preliminary estimation of the calibration curve for carbon component in the samples of the second type.

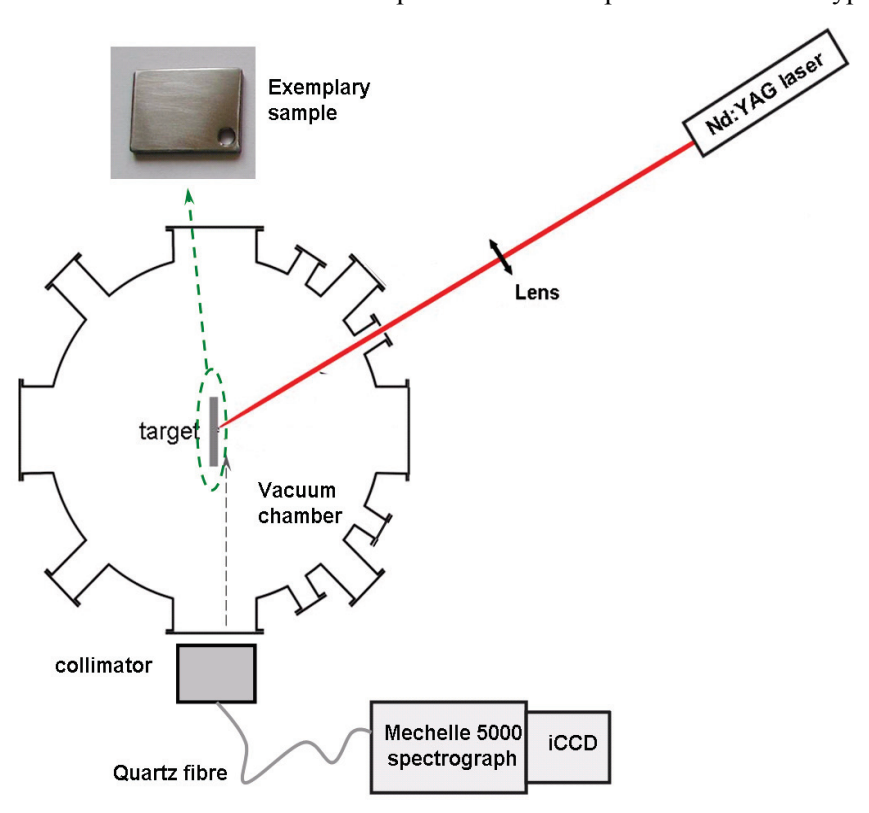


Fig.1. Experimental set-up

The results can be divided into two parts in regard to the type of the samples. For both types the spectra for subsequent shots and series of shots were recorded in order to observe the spectra evolution for removal of the layers. In the case of IU-90 type of samples the spectra obtained during subsequent shots indicated presence of 4 zones in the sample depth profiles with specific features which may be attributed to different layers and they boundary areas. The spectra are presented in figure 2.

Based on the integration of the curve intensities it was possible to estimate the spectroscopic depth profile of the sample. The profile is presented in figure 3 and is consistent with the GDOS profile provided by the manufacturer.

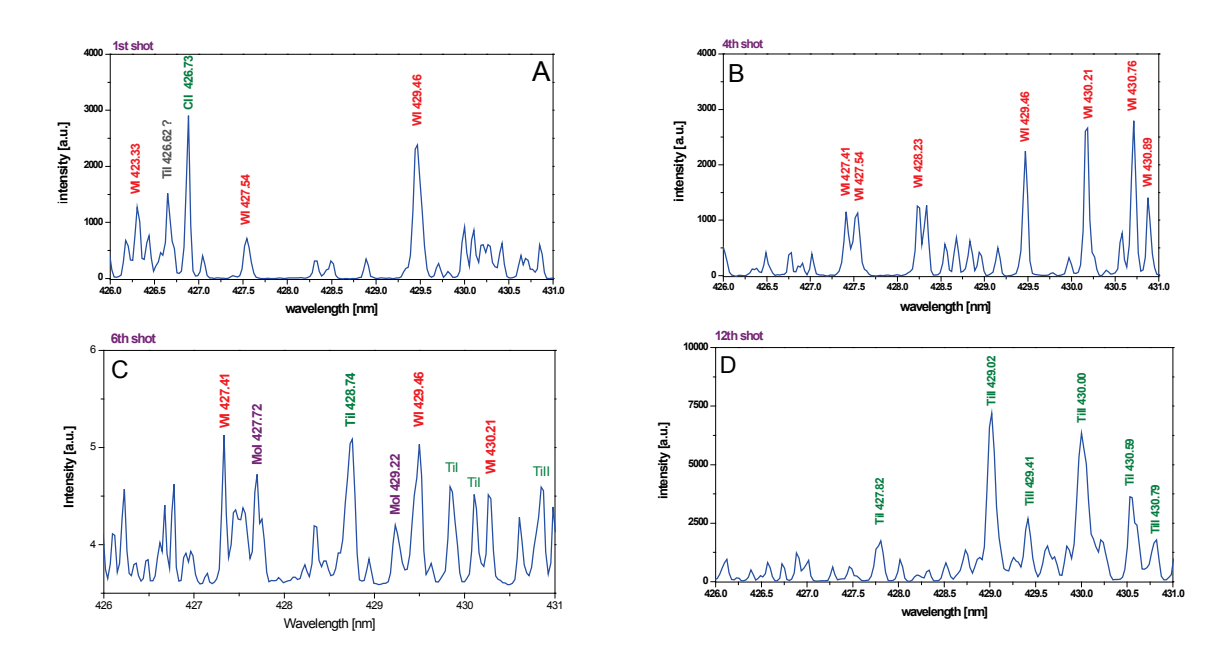


Fig. 2. The spectra obtained for: A) Contaminated surface layer B) tungsten layer C) Through the molybdenum interlayer D) Titanium substrate

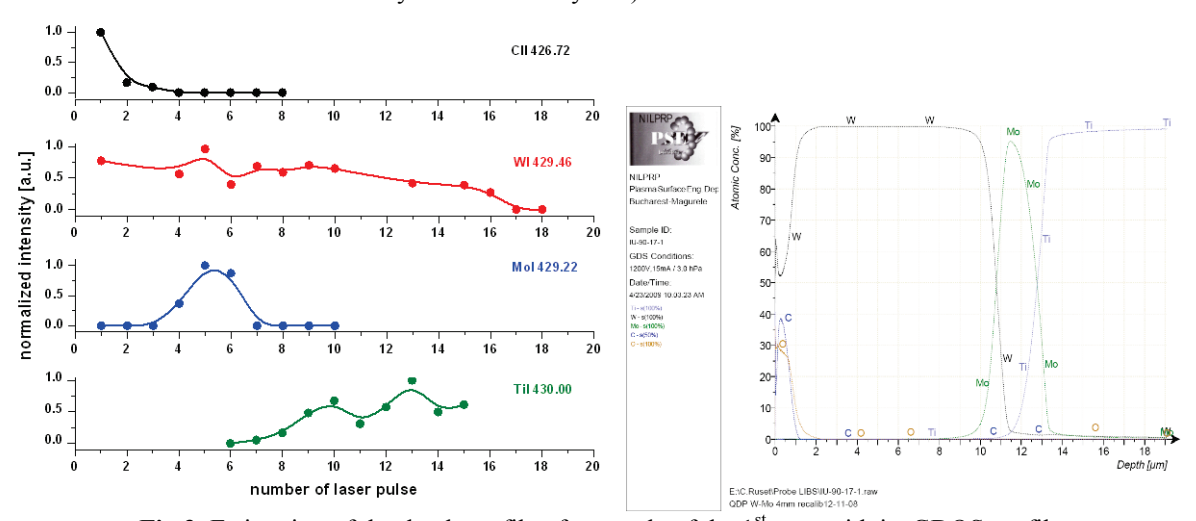


Fig.3. Estimation of the depth profile of a sample of the 1st type with its GDOS profile

After preliminary experiments which were aimed at identification of most distinct spectral features and optimization of the set-up, the arrangement and parameters of the experimental set-up have been set and a narrow band of the spectra have been chosen for further observation in the experiments for detailed characterization of the samples.

In that case the experiments were carried on with a beam of power density of 5 MW/cm². In case of the presence of carbon it was important to adjust a proper value of time delay which had to be short enough to observe recombination of speedily propagating carbon ions. The delay at level of 200 ns was not short enough and the time as short as 100 ns was needed. During subsequent shots up to the shot no. \sim 16 (12) the spectra had a good repeatability and both ratio between intensities of the C and W lines and absolute magnitudes of the lines constant in range of \sim 10%. Around \sim 16th (12) shot the presence of titanium substrate started to be detectable.

Integration of the lines of carbon for subsequent shots, in the same irradiation and optical system collection conditions, in samples with different composition ratio of carbon allowed for the estimation of

the calibration curve for line intensity in dependence on carbon ratio in the range from 70 to 80 %. The curve is illustrated in figure 4.

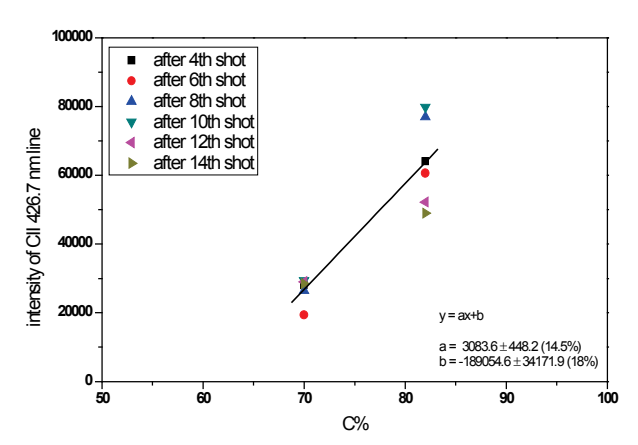


Fig.4. Calibration curve for carbon ratio in the samples of the 2nd type

The attempt for estimation of the calibration curve was a natural step in the project and although it was not very firm it was a big step forwards, because the features of the laser induced plasma appeared to be stable enough to give results in a reasonable range of confidence. The clearly difference between obtained intensities of Carbon line for both calibrate samples is seen. The reason could be a fact that the sample contained 82 % of Carbon was prepared with larger inaccuracy. The further steps should be aimed at the broadening of the calibration range for carbon (which is accompanied with co-deposition in present device) and at estimating of such curves for hydrogen isotopes which is a goal of this task itself.

The future research should also be focused on investigation of samples with calibrated contents of hydrogen isotopes which are crucial for the task. At least three calibrated samples with different composition of Carbon, tungsten and Hydrogen (Deuterium would be more convenient) should be investigated.

Study of laser based diagnostic methods, photonic cleaning and spectroscopy (including LIBS) in perspective of next-step fusion devices (including ITER)

The work conducted included activities of the DLP IPPMM in the area of the following EFDA-DTM tasks:

- WP1.1 DEM system: to perform a review of possible laser-based techniques which could be employed together with a detailed feasibility study for the possible integration on ITER,
- WP1.3 To review the spectroscopy diagnostics foreseen on ITER to check their adequacy for erosion measurements
- WP2.1 To assess the possibility of using a photo-cleaning method for removing the dusts deposited on the divertor surfaces

For development of the DEM system the following techniques have been taken into account:

- LIDAR method in the basic set-up or with modifications (Doppler based or with heterodyne optical detection).
- Speckle interferometry in different configurations (basic, two/multi wavelength, with extended range),
- Time resolved spectroscopy
- Industry solutions as Laser scanning Inspection.

The analysis of the advantages and drawbacks of the methods led to the conclusion that the most favorable method is two-wavelength speckle interferometry with heterodyne detection (fig.1) which

seems to be the most powerful and the best documented among other methods. Other techniques often suffer from fundamental restrictions which are too tough to match sophisticated ITER requirements (which looks to be true for LIDAR methods). Another issue is the problem of vibration for which the interferometry with further signal processing seems to be the most reliable method to deal with. The method based on the novel timed-resolved spectroscopy approach was rejected due to many uncertainties regarding which solutions would need effort exceeding the framework of the task. The industry offer, however reliable, seemed not to offer enough flexibility to be applied in harsh fusion reactor environment.

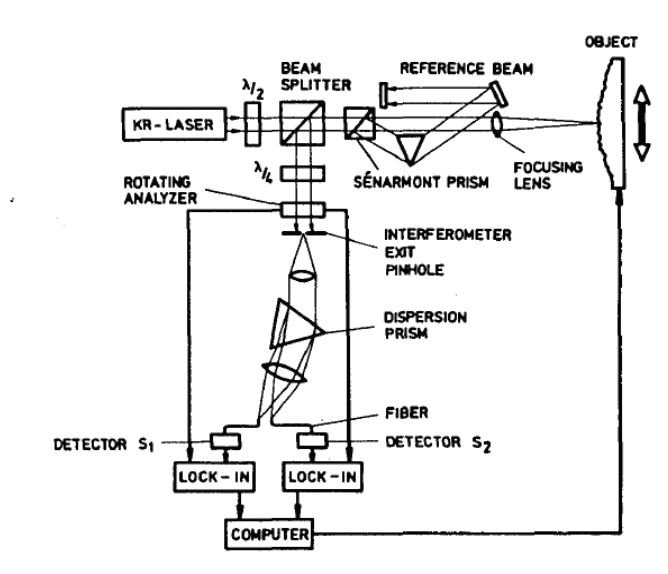


Fig.1. A sample set-up of a 2-wavelenght speckle interferometer with heterodyne detection [A. F. Fercher, H. Z. Hu, U. Vry, Applied Optics, **24**, 2181 (1985)]

The study aimed at adopting of the spectroscopic diagnostics foreseen for ITER for measurements of erosion was based on the consideration that the erosion yield can be estimated on particle fluxes which can be calculated based on spectroscopic measurements. The research must have started from defining spectral ranges for observation of the lines which calculations could be based on and the proposing the solution of the diagnostic systems foreseen for ITER which would be convenient for realizing measurements of the lines. As a system which would possibly fulfil those demands, based on the ITER diagnostics documentation, VUV spectrometer signed as PBS5.5.E.04 which has components mounted UP01, E01 and D02 has been chosen. The system is designed collect light form 200-1000nm range for monitoring the impurities. Further study on the parameters of the system and requirements to yield the information on erosion is in progress.

The research on the assessment of possibility of using a photo-cleaning method for removing the dusts deposited on the divertor surfaces was based on the experience gained in the framework of other projects. The subject of the study was a removal of the layers and dust mobilization from deposited surfaces of invessel tokamak components and calibrated samples with the use of Nd:YAG and Yb:fiber laser system working in different ranges of power density.

The investigated samples (taken from tokamaks or calibrated samples prepared by collaborating institutes) are mounted in the vacuum vessel at the pressure of 5x10-5 mbarr or 3 Pa depending on the series and goal of the experiments. The samples are subjected to laser irradiation of power density which is controlled with the use of the focusing lens mounted outside the vacuum chamber. For real time characterization of the process Laser Induced Breakdown Spectroscopy, ion diagnostics (ion collectors and electrostatic ion energy analyzer) and CCD camera are used. Besides the application of the real time diagnostics, the effects of laser treatment have been tested with techniques of material research (QMS, profilometry, SEM, TEM, NRA) which generally confirmed removal of the deposits from the surface of tokamak components and also gave evidence of presence of fuel particles in dust mobilized from the surface. In the recent experiments there was also Yb: fiber laser used which delivered pulses of lower

power density but the average power of the system was significantly higher (up to 100 W at repetition rate of 100 kHz).

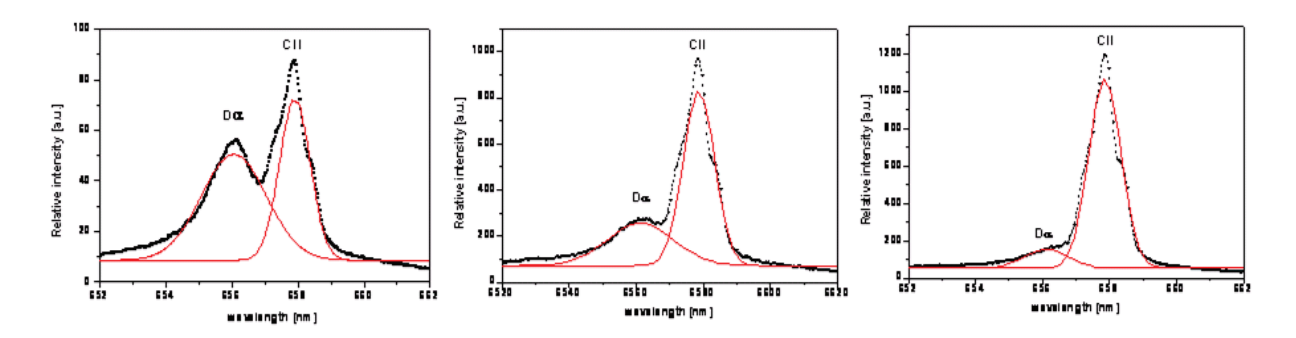


Fig.2. Illustration of removal the deposit from the TEXTOR limiter sample, spectra for 5, 20 and 40 shots, respectively.

In general, the study leads to conclusion that removal/mobilization is easy to be obtained with the use of laser irradiation (fig.2), both for thick or thin deposits, but still optimization of the process regarding the application is needed.

Laser-induced removal of fuel and co-deposits from plasma facing components in tokamaks.

Characterisation of gas, plasma and dust released from laser-irradiated samples and investigation of laser-irradiated surface of samples

A removal of the in-vessel deposited layers by the means of both laser removal or ablation is a candidate method for dealing with fuel retention in next step tokamak devices. The experiments carried out at DLP IPPLM in the previous years led to optimization of the ablation method for deposits present in carbon-based devices. Due to an increasing role of the metallic components (tungsten and beryllium) as candidate materials for the next step devices the need appeared for detailed investigation of the removal of layers containing these elements. As in case of carbon based materials, the issue of utmost importance was not only to optimize the method but also to develop a real time diagnostics for monitoring it. The works were supported by the experience gained while developing previous tasks and were based on spectroscopic and ion diagnostics which were adopted to the experiments on mixed material samples from diverse collaborating laboratories.

In the experimental set-up as the irradiation source the Nd:YAG laser system which delivers 3 ns pulses of up to 600 mJ at 1064 nm was applied. The beam was focused on the target, which was mounted on the movable holder in the vacuum chamber at pressure of 5x10⁻⁵ mbarr or 3 Pa depending on the series of the experiment, with the use of the lens of focal length of 80 cm. The distance between the lens and the target was different in subsequent experimental series and was subject to optimization in terms of power density for the fastest removal and efficient collection of the measured optical signal. The light signal was collected by the means of collimator mounted outside the vacuum chamber at the distance 40 cm from the target. The area of observation of laser-induced plasma was a circle of the diameter of ~5 mm distanced ~3 mm from the target. The light emitted from this area was observed in the direction parallel to the target. The collimator was connected to the Mechelle 5000 spectrometer with the 50 μm core silica fiber. The collected signal was amplified by the ICCD and recorded by the means of SOLIS software. The acquisition system was triggered by the standard TTL signal from the laser system. The delay after laser shot was adjusted based on the features of the investigated samples and aims of the observation.

Depending on the goal of the experimental campaign, different types of samples were under investigation, namely:

- for investigation of a removal of the deposited layer from in-vessel mixed-material components: samples of AUG divertor from the inner and outer strike point region partially covered with thin co-deposit layers. There were three types of samples of this kind: a) graphite substrate with PVDed 4 μm W coating, b) graphite substrate with plasma sprayed 200 μm W coating, c) graphite samples without any coating,
- for spectroscopic investigation of removal of mixed-material layers from calibrated samples: samples with diverse concentration of C, W and Al (as beryllium analogue) prepared by IEMT, Warsaw, Poland
- for investigation of the film break-up process by the means of fast CCD camera and preliminary experiments with thick co-deposite removal with the high power fiber laser: ALT TEXTOR limiter sample with ~40 µm co-deposited layer on the deposition zone.

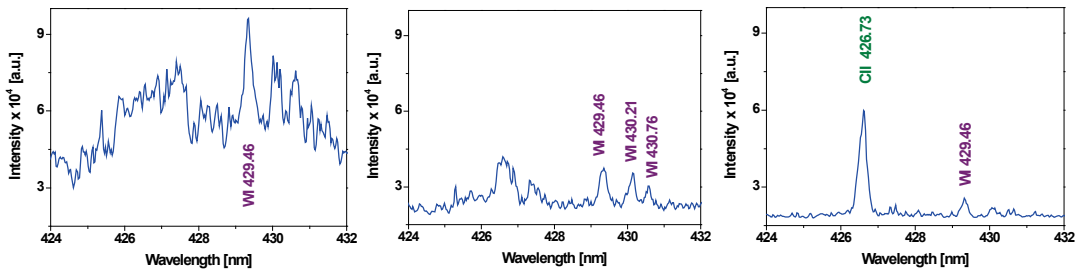


Fig.1. Spectra taken for AUG sample with 4µm tungsten layer, after 1st, 4th and 7th laser puls, respectively

The results of the investigation of AUG samples (which was a continuation of the research started in 2008) confirmed the presence of fuel particles in a thin film on the samples and allowed for the choice of a narrow wavelength range which was very convenient to track the chemical ratio between components of the sample. Sample spectra obtained different subsequent phases of the removal process are shown in figure 1.

Integration of the lines allowed for estimation of the depth profile of the samples. A representative one is given in figure 2.

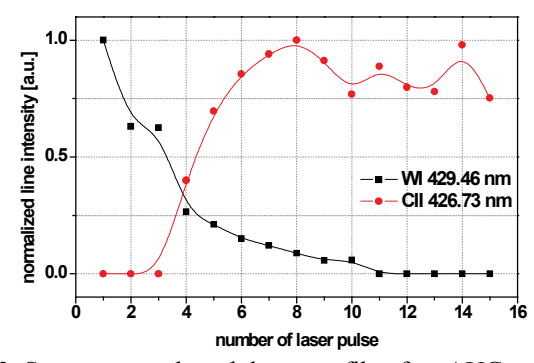


Fig.2. Spectroscopy-based depta profile of an AUG sample

The results of the optical spectroscopy were thoroughly consistent with the results obtained for the samples with the use of electrostatic ion energy analyzer (IEA). Basing on the very precise ion measurements it was possible to observe that deuterium and other contamination (C) are present only on the very surface of the tungsten coated samples.

Promising results were also obtained in tests of the fiber laser for fuel removal. First experiments used Yb:fiber as a irradiation source for removal and Nd:YAG pulses as a source for generation of plasma for LIBS before and after the irradiation by the fiber laser. The results, which are presented in figure 3, clearly indicate that after 1 s irradiation by the fiber laser, the fuel particles were completely removed from the target surface.

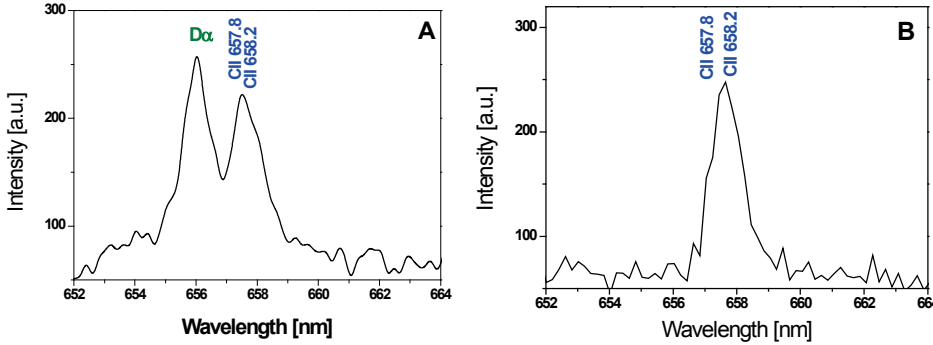


Fig.3. Optical spectra of trick TEXTOR co-deposite A) before and B) after 1 s irradiation with the Yb:fiber laser

Another experiment with Yb:fiber laser was conducted to test a possibility of "dustless" fuel removal. At this end a cylindrical aluminum dust collector (which was used in previous experiments at IPPLM) was mounted in front of the target plate. The collector has a drilled top to transmit the fiber beam with ability to collect most of the dust generated during the interaction process. In some previous experiments the dust successfully collected this way in the form of both macroscopic particles and deposited on its walls in a film of microscopic/nano particles was investigated in several collaborating laboratories. In the preliminary experiment with fiber laser no macroscopic particles of dust were found in the collector which may indicate that the removal process with this laser can lead to removal without further fuel retention in dust particles released during the process.

Studies of material erosion and re-deposition on plasma facing components from the present day machines. Characterization of exposed PFCs with various microscopic and analytical techniques (TEXTOR and AUG)

The investigations carried out in 2009 included:

• Post mortem analysis of tungsten coated tiles from the divertor strike point region of AUG - 2007 campaign (TEM examinations of deposits developed at these tiles and bubble-like elements present at the surface of tungsten coating exploring FIB technique).

It has been generally observed that the coatings were modified by high-heat loads and co-deposition of species from plasma. STEM/TEM examinations of the inner divertor strike point tile revealed deposit, up to 1.5 µm thick, of characteristic stratified structure. The deposit material was compact, however, seldom voids were present. The observed sub-layers differed in thickness (10-50 nm), structure and chemical composition. The EDS analyses showed that the main elements of the deposit were carbon, tungsten and oxygen. It was observed that the part of deposit closer to the coating surface was richer in carbon in comparison to the external one. The diffraction patterns proved deposit amorphous character. In the case of outer strike point region the observations revealed large areas subjected to erosion as well as blisters formation in the cavities of the coating. Much thinner deposit, on average 60 nm thick, was revealed.

• Examinations of dust originating from TEXTOR and AUG (observations of dust size and morphology by SEM and examinations of their chemical composition by EDS; examinations of dust internal structure by FIB and TEM).

The SEM studies revealed that dust particles differ in their chemical composition and morphology/size. The particles size was in the range from several microns to submicron size. Different particles morphologies were observed and described.

The AUG dust particles were catalogued into four groups: (1) carbon based (60% of examined debris), (2) C-O-Si particles, (3) metal-based and (4) fine particles. In the case of TEXTOR dust C-O-B mixed, metal-based, ceramic and fine particles were detected.

A large number of fine particles (micron and sub-micron size) was revealed on the surface of larger ones. Some of them were small fragments of carbon based fakes, a large fraction, however, was metallic,

Physics and Technology of Fusion

predominantly tungsten based. Frequently particles rich in iron and chromium as well as silver were detected. Fine ceramic particles (Si, Al, O) were also present.

 Characterization of the plasma-induced damage in TEXTOR Langmuir probe (observations of probe morphology by SEM and examination of its chemical composition by EDS)

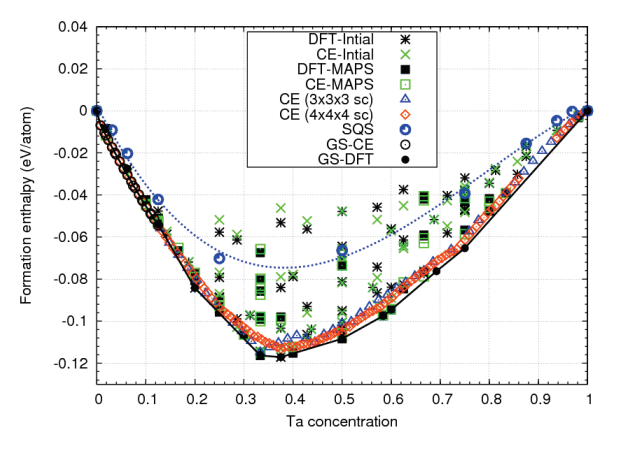
During the experimental campaign, the tip of the probe was partially melted, evidence of this event is visible in the form of re-melted tungsten droplet. At the surface of the probe the fine flattened droplets, up to 150 µm in diameter were observed. The EDS measurements revealed that they were rich in aluminum and oxygen. One can assume that they originate from the fragments of alumina insulation of the probe. In the overheated region, adjacent to the re-melted part of the probe, the probe material (tungsten) re-crystallized. In the area with fine alumina particles the probe surface was locally lightly remelted. No evidence of blisters formation was found.

	Physics	and Te	chnology	of	Fusion
Davida		of 100	مامناما		
Develo					
and adv	anced i	mater	ials for	DI	EMO

Ab-initio study of defects configurations and their interactions in W-Ta and W-V model alloys

In the study, the phase stability of tungsten-based alloys W-Ta and W-V, the structure and formation energies of radiation defects in these alloys were investigated.

Using ab-initio calculations, enthalpies of mixing for large sets (~100 structures) of alloy configurations, considering several alternative ordered structures corresponding to the same chemical composition were compared. In this way the lowest energy intermetallic compounds that are expected to dominate alloy microstructures (the so called Ground State structures), and hence the low temperature part of phase diagrams, for both alloys were identified. For both alloys in tungsten rich concentrations (up to 12.5 % Ta and 20.0 % V) of alloying element the GS structures can be formed. There are about 20-30 GS structures in the W rich concentrations (see Figs. 1 and 2). It is worth noting that these structures form solid solutions, which is important information for alloy design as in these concentrations the usually brittle intermetallic phases cannot be formed.



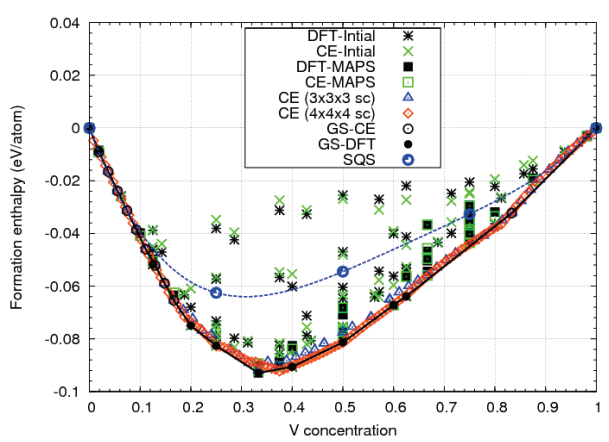


Fig. 1: Enthalpy of mixing vs. Ta concentration calculated using DFT and CE (GS structures marked with black dots and circles)

Fig. 2: Enthalpy of mixing vs. V concentration calculated using DFT and CE (GS structures marked with black dots and circles)

Size effect of alloying element was also studied for WTa and WV alloys. The W, Ta and V have different atomic volumes 15.78, 18.12 and 13.77 ų, respectively. In ideal solid solution the volume per atom is a linear combinations of alloying element concentrations (Vegards law). The volume relaxed configurations of alloys with those given by Vegard's law were compared. It was found that W-V alloys exhibit almost no structural relaxation. Contrary, in the case of WTa alloys significant difference was notted. This allows to conclude that the WV alloys form structures very close to bcc one wheras WTa ones form phases that have highly deformed crystal lattice compared to bcc. It is particularly important in the context of mechanical properties of these alloys. The bcc structures have high symmetry and much more slip system than distored ones, therefore WV alloys shall exhibit much higher plasticity in comparison to WTa alloys.

Ab-initio calculations also show that vanadium atoms strongly trap self-interstitial atom defects in W-V alloys, whereas Ta atoms in W-Ta alloys have very little effect on either the formation energy or thermally activated mobility of self-interstitial atom defects.

Development of W-EUROFER based on PPS and a transition layer incorporated between both materials to decrease thermal stresses

The experiments concentrated on fabrication of tungsten-to-Eurofer steel joints by pulse plasma sintering (PPS) technique. Low activation elements were used for transition layers between the joined materials in order to mitigate large difference in thermal expansion coefficients of W and steel and reduce the resulting thermal stresses at the joint interface. Four different materials were tested (pure iron and titanium as well as two Fe-Ti compounds). Carried out experiments allowed establishing optimal PPS sintering parameters for those materials. It was shown that interlayers incorporated between W and

Eurofer 97 steel were characterized by low porosity and well adhering to both joined substrates. Simple thermocycle tests consisting of the samples heated to the temperature of 700° C and annealing for 15 min and following rapid cooling in room temperature water allowed identification of the promising interlayer (see Table 1). The interlayer made of pure α iron was the one with the highes resistance to the thermocycle test performed. One of the joints sustained 30 cycles i.e. the assumed maximum.

Tab. 1 . Results of the thermo	vcle tests of the	W/Eurofer 97	ioints
---------------------------------------	-------------------	--------------	--------

	Sample number	Number of tests passed before delamination
	1	10
W/86FeTi/Eurofer 97	2	10
	3	12
	1	18
W/Fe/Eurofer 97	2	24
	3	30 (test passed)

Hydrostatic Extrusion (HE) processing of ODS ferritic steel: microstructure characterisation, mechanical properties and thermal stability

The microstructure and mechanical properties of an oxide dispersion strengthened (ODS) reduced activation ferritic (RAF) Fe-14Cr-2W-0.3Ti-0.3Y2O3 steel fabricated by hot isostatic pressing (HIP) followed by high speed hot extrusion (HSHE) and heat treatment (HT) at 1050°C were investigated. Transmission electron microscopy (TEM) revealed significant differences in grain size and dislocation density of as-HIP ped and as-HSHE materials, the latter being characterized by smaller grains and larger dislocation density. Heat treatment performed after HSHE and subsequent microhardness measurements revealed that ODS steel is stable up to the annealing temperature of about 1250°C. After annealing at a temperature of 1350°C the microhardness decreases by about 30% from 460 to 330 HV0.1. These results suggest that recovery and recrystalization processes occur at the temperature higher than 1250°C which is in a good agreement with microstructure observations and the literature data. It should also be noted that the grain size remains almost unchanged upon annealing up to 1250°C. Annealing at 1350°C results in the volume fraction of the coarse grains being increased from 10 up to 25%. This indicates that the pinning of the grain boundaries by oxide nanoparticles is effective up to 1250°C.

It was demonstrated that the HSHE process significantly improves tensile and Charpy impact properties of the ODS steel. Tensile strength at room temperature increased from 950 MPa up to 1350 MPa. Also Charpy impact properties, especially upper shelf energy, significantly increased (from 3.0 up to 6.0J - see Fig. 1). Ductile-to-brittle transition temperature (DBTT), even though improved in comparison to as-HIPped specimen, remained however relatively high (about 75°C).

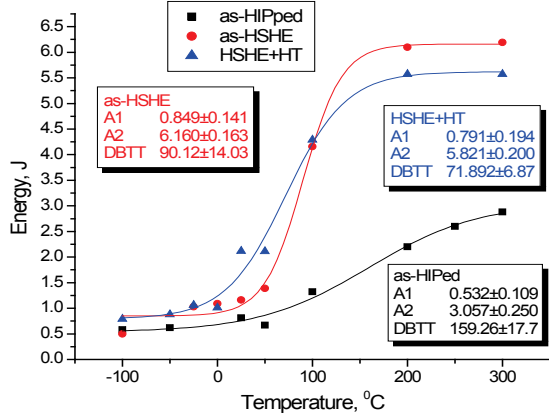


Fig. 1 Charpy impact properties of the ODS ferritic steels in various stages of the process

Physics and Technology of Fusion
Fusion plasma diagnostics

Activation technique in a cross-check experiment for high resolution neutron spectrometer

The aim of the project was to assess the feasibility of application the activation method to cross-calibrate High Resolution Neutron Spectrometer.

The activation technique has been used at JET for the time-integrated measurements of neutrons on time-of-flight spectrometer (TOFOR) line of sight (KM11 LoS). The indium samples were placed at the vertical collimated line of sight above TOFOR spectrometer. Their dimensions had been optimized with LabSOCS software for gamma-activity measurements by means of our HPGe spectrometer.

Several series of irradiations of the samples have been performed. The gamma activities for $^{115}\text{In}(n,n')$ ^{115m}In and $^{115}\text{In}(n,\gamma)$ 116m In reactions have been measured by means of HPGe detector.

The results of measurements at KM11 LOS using for described below calculations are presented in the Table 1.

Table 1.

Discharge number	Reactions	Decay constant [s ⁻¹]	Activity [Bq]	Neutron yield KN1 -Y _n	Sample mass [g]
76060 - 86	$^{115}In(n,n')^{115m}In$	4,29·10 ⁻⁵	15,8	$4,47\cdot10^{17}$	9,14
	115 In(n, γ) 116m In	2,13·10 ⁻⁴	7,65	1,67·10 ¹⁷	,
76748	¹¹⁵ In(n,n') ^{115m} In	4,29·10 ⁻⁵	1,46	1,61·10 ¹⁶	132
70710	115 In(n, γ) 116m In	2,13·10 ⁻⁴	2,39	1,61·10 ¹⁶	1.52
76914-917	¹¹⁵ In(n,n') ^{115m} In	4,29·10 ⁻⁵	4,18	6,83·10 ¹⁶	132
70711711	115 In(n, γ) 116m In	2,13·10 ⁻⁴	4,98	4,42·10 ¹⁶	132

The measured activities have been used as an input in the calculations of a fraction of low energy (0-0.4MeV) and high energy (0.4-14MeV) neutrons.

The activity of the i^{th} radioisotope generated in the volume element dV_D of the indium target due to primary neutrons emitted by volume of plasma dV_P , at the limited time after **n** pulsed irradiation can be written as

$$dA_{Pi,n} = \lambda_i dN_T \langle \sigma_{ai} \varphi_P \rangle \sum_{j=1}^n \delta \Psi_{Pj} e^{-\lambda_i T_j}$$

where dN_T – the number of target nuclei contained in the volume element dV_D

Integrating above eq. over all the volume V_D of the In target and over all the effective volume V_{P0} and including geometrical factor, the activity of the i^{th} radioisotope generated in the target due to primary neutrons is given:

$$A_{Pi,n} = \lambda_i N_T \langle \sigma_{ai} \varphi_P \rangle G_F \sum_{i=1}^n Y_j e^{-\lambda_i T_j}$$

In which G_F is a geometrical factor related to angular dependence of the neutron emission from the plasma element dV_P (for isotropic emission $f(\Omega) = 1$) and the exponential accounts for primary neutron attenuation along the path d.

We can denote that total activity $A_{i,n}$ of the i^{th} radioisotope generated in the target, i.e., the activity due to primary and secondary (scattered) neutrons was measured. So, we can consider this fact by the term

 $\langle \sigma_{ai} \varphi \rangle$ where φ is a total neutron distribution, i,e., the distribution including primary and secondary neutrons.

So, we can rewrite the formula of total activity in the following way:

$$A_{i,n} = \lambda_i N_T F_{Ai} F_{Spi} \langle \sigma_{ai} \varphi \rangle G_F \sum_{i=1}^n Y_j e^{-\lambda_i T_j}$$

where: F_{Ai} and F_{SPi} determinate scattering corrections.

As an example the results for Pulse #76748 are shown in Fig.1.

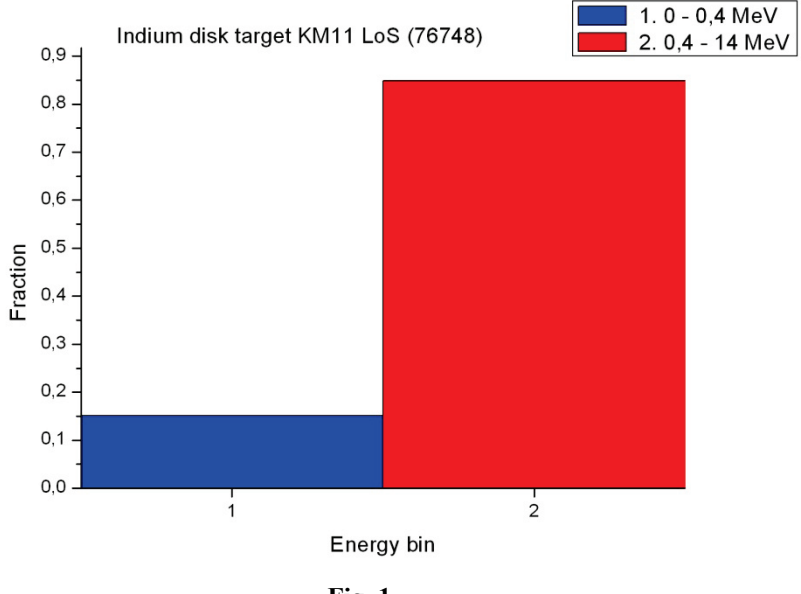


Fig. 1.

In the light of the results obtained in this work it seems possible to draw the following conclusions:

- 1. The KM11 LoS collimating system cut the low energetic part of neutrons (0, 400 keV) sufficiently.
- 2. <u>A comparison between the rough data presented in this report and MCNP calculation for the KM11 LoS collimating system can be interesting.</u>
- 3. At this point we conclude that the rough analysis is not useful for evaluation of low angle scattered neutrons in the collimating system.
- 4. In order to evaluate low angle scattered neutrons in the system the radio-nuclides with steep like cross section near 2.5 MeV ought to be used.

It seems possible to draw a conclusion that the KM11collimating system cut the low energy neutrons (0-400 keV) sufficiently. The experiment also showed that the activation method can be used to cross-calibrate a High Resolution Neutron Spectrometer. Neutron flux density determined by the activation method can be a benchmark for HRNS.

Diamond and track detectors to detect escaping fast alpha particles

Measurement of escaping alpha rates to the first wall is of great importance in planning tokamak fusion reactors. The conditions prevailing within the torus are not compatible with conventional diagnostic methods, hence the need to seek new solutions and materials that will be resistant during a tokamak operation.

Methods of measurements by the diamond and plastic track detectors are based on entirely different physical principles depending on different properties of the two materials. The methods and the obtained results are shown below in two separate parts.

Part.1 Diamond detectors to detect escaping fast alpha particles

An α detector has to be placed with no screening because of a very low range of these particles in the matter. That means the work in the extremely hard conditions in tokamak. Semiconductor detectors can be used for the spectrometric α measurements; as silicon detectors, for example. However, silicon can be easily damaged in high flux and high temperature environment. Diamond detectors have strong advantages for use in applications for α particle detection in such an environment. In this case it is a better material for detecting high energy particles, like α particles, neutrons, electrons and others.

Diamond possesses some of the most extreme physical properties of any materials and such properties as its radiation and corrosion resistance, large band gap, high electron and hole mobility make it an attractive semiconductor detector used of spectroscopy in real time measurements. Diamonds, as detectors of high energy α particles, within the operating reactor chamber, in special diagnostics ports, prove more efficient and resistant than the silicon or germanium detectors.

The diamond detector (manufactured by the Diamond Detector, Ltd.) is a high purity single crystal plate that has a thickness $0.05~(\pm0.01, -0.02)~\text{mm}$, size of $2.5~\text{mm} \times 2.5~\text{mm}$ ($\pm0.01~\text{mm}$) and gold contacts of the thickness of 20 nm. The active diameter of the diamond detector is 1.9 mm and the diameter of the detector together with housing is 27 mm. The silicon detector is a crystal plate that has a thickness 0.5~mm. The diameter of the detector without housing is 10 mm, the diameter of the detector housing is 20 mm. In a vacuum chamber, the energy calibration of the diamond and silicon detectors has been performed in order to compare results of the measurements with the diamond detector to those with a known silicon detector. The radioactive source 239Pu 241Am 244Cm (PAC) has been put directly on the surface of the detector in a vacuum chamber. The α spectra acquired using the diamond and silicon detectors are shown in Fig. 1

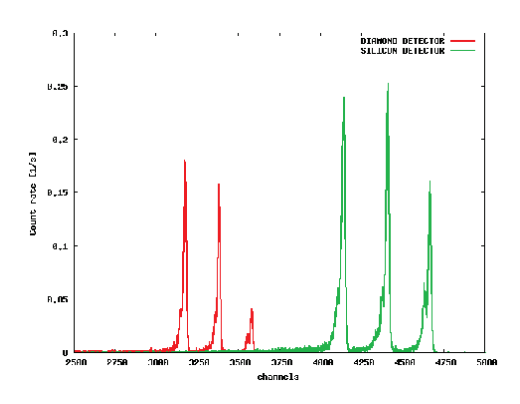


Fig. 1.

The PAC source emits α particles with three main energies, therefore three corresponding peaks are clearly visible in the spectrum. There are other small peaks that appear at the left hand side of the main peaks due to small contributions of α particles emitted by the PAC source with smaller energies.

The monoenergetic ion beam measurements have been carried out in a laboratory of the Institute of Nuclear Studies (Otwock-Swierk, Warsaw Branch, Poland). The Van de Graaff accelerator has been used to accelerate the once-ionized helium ions (${}_{2}^{4}$ He $^{+}$) to obtain finally monoenergetic beam of the α particles. The beam of ions has fallen on a scattering foil held by two handles. Only the ions scattered back under the angle γ (30°) have been detected.

The following incident energies E0 of the ion beam have been used: 400 keV, 1000 keV, 1500 keV and 2000 keV. In Fig. 2 are presented the energy spectra of helium ions ${}_{2}^{4}$ He $^{+}$ scattered on the gold foil of 100 μ g/cm 2 recorded with the diamond detector.

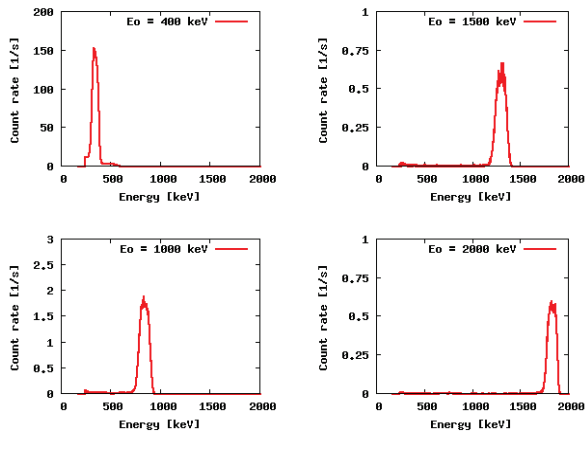


Fig. 2.

Linearity of the amplitude signal has been investigated. In Fig. 3, the measured peak energy values Em are plotted in function of the known values of the scattered helium ion energy E1 and peak positions Et of the PAC source. All the points lie perfectly on the same calibration line, which is obtained from measurements with the monoenergetic beams only.

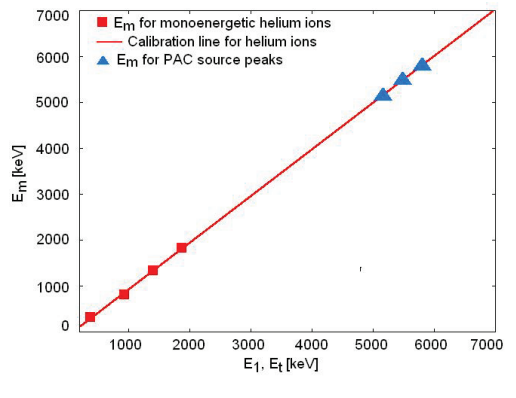


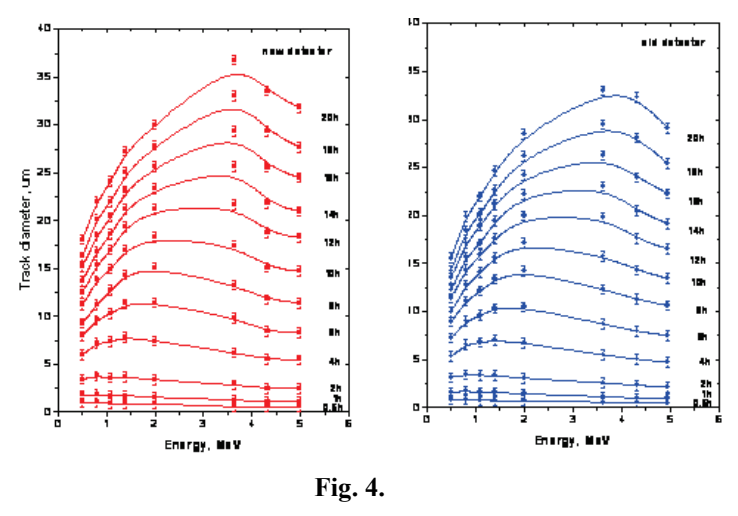
Fig. 3.

The carried out experiment has been an introductory for measuring spectrometric properties of the diamond detector used for the α spectrometry. A very good energy resolution has been observed, comparable with the silicon detector resolution. The observed linearity of the energy measurements in the range investigated (0.4 to 2 MeV and extended to 5.8 MeV) is a very important property of the diamond detector. Future measurements of the lost alphas energy below 3.5 MeV at tokamaks will be significant for the thermonuclear plasma diagnostics. More careful test experiments are expected in order to find out which factors influence the results of the measurements for pure α beams and with presence of other radiation (γ , n, t, d) expected in a real surrounding of tokamaks.

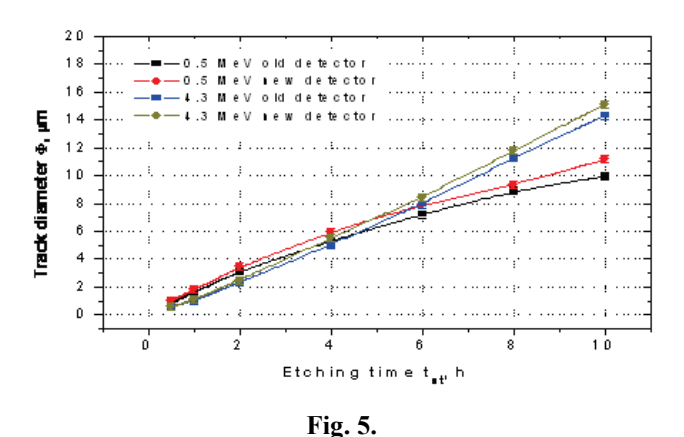
Part.2 Track detectors to detect fast alpha particles

In order to perform detailed calibration measurements of the purchased detectors, selected samples (cut from the detector sheets delivered in both of the batches) were irradiated with mono-energetic 4He ions of different energies provided by a particle accelerator. During these irradiations the ion energy value was changed in steps of 200 or 300 keV in the energy range from 500 keV to 5 MeV, and different samples were irradiated with 4He ions of various energies.

The calibration diagrams showing track diameters as a function of 4He ion energy and etching time, as found in this work, are presented in Fig. 4



The diagrams demonstrate specific maxima, which appeared to be considerably wider and shifted to higher energies than similar maxima determined earlier for protons' and deuterons' calibration diagrams. The track diameter evolutions, expressed as a function of etching time are presented in Fig. 5.



Each curve in this figure describes the evolution of diameters of the craters induced by 4He ions of the same energy. The detection diagrams shown in Fig. 5 reveal that diameters of etch-pits, which were produced by mono-energetic 4He ions, increase linearly versus etching time within a certain range of this time. A critical value of etching time is that at which an external layer of the detector equal to the ion range in the detector material is removed by the bulk etching process.

Cherenkov detectors for fast electron measurements: new diagnostics for Tore-Supra

The detectors based on the Cherenkov effect, which were developed and manufactured at IPJ in Swierk in the previous years, enabled for the first time direct measurements of fast electrons within the TORE-SUPRA facility at CEA-Cadarache (France) to be performed by the end of 2008. The recorded electron-induced signals were analyzed in 2009. Taking into consideration a complicated geometry of the experiment and possible configurations of the fast electron beams appearing within the so-called scrape-of-layer (SOL) region, it was decided to design and manufacture a new Cherenkov-type measuring head of a modified construction which could be fixed to the movable probe. That probe was for the first time applied for measurements within TORE-SUPRA during the recent experimental campaign in March 2010.

In a frame of experimental studies of fast electrons within the ISTTOK facility in Lisbon (Portugal) the series of measurements by means of a four-channel Cherenkov probe, which made possible estimations of electron energy ranges, were performed. Simultaneously, there were performed measurements of hard X-rays (HXR), which enabled some correlations with the fast electrons to be determined. In order to get stronger electron signals and to expand the investigated energy range two new Cerenkov-type measuring heads were designed and constructed, each equipped with four radiators made of aluminium nitride (AIN).

The most important results of the studies, carried out in 2009, can be summarized as follows:

• TORE SUPRA. The electron-induced signals, recorded by the end of 2008 (during the first experimental campaign), had been carefully analyzed by the beginning of 2009. Principles of the applied measuring technique, the construction of the applied Cherenkov-type probe, as well as some results of the performed electron measurements had already been published in the Review of Scientific Instruments. The obtained time-resolved signals were short in time (they lasts about few milliseconds), and their intensity was very low (about 10 mV). These signals could be recorded only by means of a fast digital oscilloscope, and not by a standard data acquisition system of the TORE-SUPRA tokamak. Small signals, which were obtained also from two channels only, might be explained by the shadowing of the radiator tips by a projection of the CFC shield edge. The main conclusion was that the quasi-stationary electron layer was observed. Its thickness was estimated to be about 1-2 mm; but one cannot exclude that the electron layer thickness may be larger because the Cherenkov probe could not record the whole electron layer for geometrical limitations.

It was decided to design a new Cherenkov-type measuring head of a modified construction. The main idea of modification was to move the positions of radiators from the side surface to the front surface of measuring head. The new probe was equipped with four separated diamond radiators, with Molybdenum filters of different thickness: $6 \mu m$, $21 \mu m$, $39 \mu m$, and $60 \mu m$. They enabled to record the fast electron beams with following minimum energies: 72 keV, 111 keV, 151 keV, and 191 keV.

In January 2010 the new detector was assembled upon the internal reciprocating shaft (the same as in 2008). The new Cherenkov probe was finally applied for electron measurements within the TORE-SUPRA during the recent experimental campaign in March 2010. The electron-induced signals obtained during March 2010 campaign were much longer than during the first campaign, they lasted about 80-100 milliseconds. The signals were recorded for about 70 shots performed during this campaign - on the level of a few volts so the standard data acquisition system of TORE-SUPRA could be applied. The set of examplary signals is shown in figure 1.

On March 26, 2010 the measurements were performed for different plasma scenarios with Low Hybrid Current Drive heating and discharge regimes, which were especially chosen for ripple-born electrons measurements by means of the Cherenkov type detector. The shaft was moved two times during one discharge, at t = 5 sec and t = 34 sec. The obtained signals were correlated with the shaft movement and other basic plasma signals: i.e. LH heating, plasma current, and the line-averaged plasma density. The obtained results need further analysis and comparison with the results of the measurements by means of a DRIPPLE graphite collector.

• ISTTOK. The detailed measurements by means of the described four-channel Cherenkov probe enabled energy values of electrons (which arrived to the radiators) to be estimated. From a comparison of the recorded electron signals one can deduce that the most electron population had the energy between 95 keV and 120 keV.

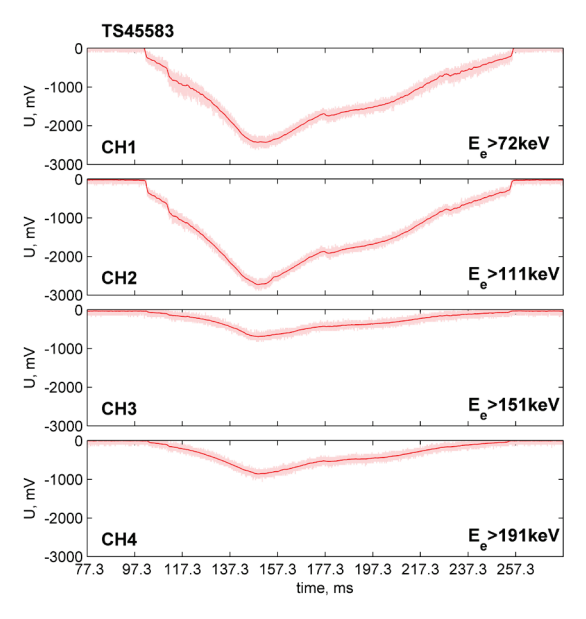


Fig.1. Set of signals from different channels of the new version of TORE-SUPRA Cherenkov detector, as recorded for TS45583 shot (start point of the time scale corresponded to $t = \sim 5.0$ sec)

The recorded Cherenkov signals corresponding to the different energy thresholds are shown in figure 2.

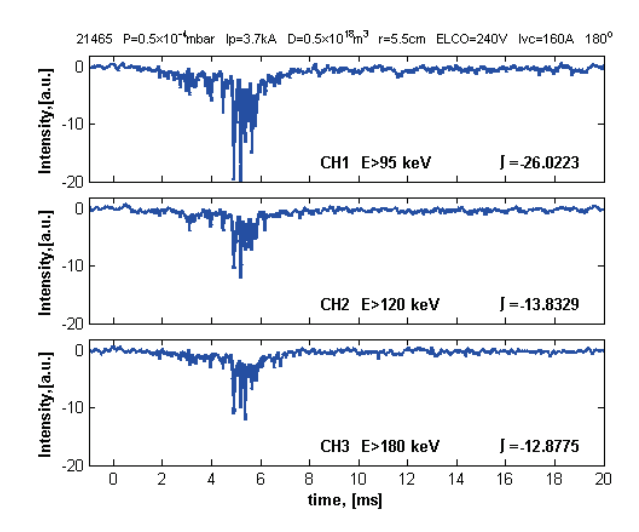


Fig. 2. Intensity of electron signals recorded in different energy channels and their integrated values (1)

The hard X-ray emission (HXR) from ISTTOK discharges was measured by means of the separate scintillation probe described above. Typical HXR signals, together with signals from electrons of energy >87 keV and a waveform of the plasma current are shown in figure 3.

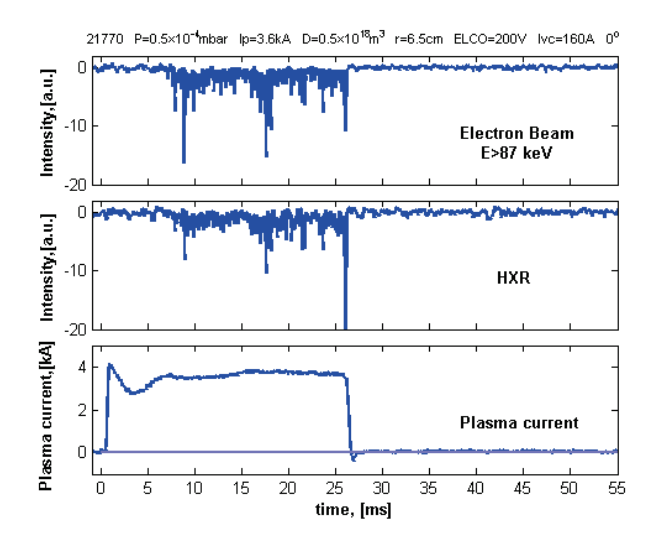


Fig. 3. Intensities of electron beams and hard X-rays (HXR) in a comparison with the discharge current waveform, as recorded for the Cherenkov probe position inside the plasma torus at r = 6.5 cm

Those observations have proved that the electron and HXR (energy ranging from ~120 to 250 keV) peaks are well correlated. The distinct HXR peaks appear only when tokamak plasma emits fast electron beams (due to run-away processes). One can deduce that the HXR emission corresponds to fast electrons slowed down (Bremsstrahlung) within the tokamak limiter and walls of the vacuum chamber.

The results of the 2009 studies led to the following conclusions:

- TORE SUPRA The new Cherenkov probe was finally applied for electron measurements within
 the TORE-SUPRA during the recent experimental campaign in March 2010. The electroninduced signals were recorded on the level of a few volts and were much longer than during the
 first campaign. The obtained results need further analysis.
- ISTTOK The application of Cherenkov-type detectors for studies within ISTTOK tokamak confirmed experimentally the emission of the run-away electrons at determined operational parameters. Some estimations of an energy spectrum of the recorded electrons were performed. Measurements of hard X-rays emitted from ISTTOK discharges, which were carried on simultaneously, and a search for their correlation with run-away electrons were also important.

High-temperature Hall sensor for future applications in measurements of magnetic field in fusion reactors

Among various models of thermonuclear reactors, the tokamak is at present recognized to be the most promising concept of a very large electric power generator. In the tokamak, plasma is confined inside toroidally shaped vacuum vessel at predefined position using special configuration of magnetic fields which are generated partly by external electromagnets and partly by plasma itself. Since the magnetic fields determine a plasma position and shape and other important plasma properties, they have to be strictly controlled. The magnetic diagnostic – a set of magnetic sensors distributed around the plasma surface - is a crucial diagnostic system of every tokamak. It has to provide the following essential information:

- main electromagnetic parameters of the plasma, such as plasma current and internal inductance,
- position and speed of the plasma mass centre,
- shape of the plasma boundary, amplitude and mode number of fluctuations with frequencies ranging from quasistatic to fast.

Information provided by the magnetic diagnostic is exploited in most machine control loops and also in most other diagnostics. The close vicinity of magnetic sensors to thermonuclear plasma imposes

significant physical constraint on the magnetic sensors. For a long-pulse, long-life and high-fluence thermonuclear generator, like ITER, during its action, neutron, gamma and plasma heat loads are very large. Thermal cycling and radiation damage are also harmful for the sensors. Hence, the maintenance of sensors inside or in the vicinity of ITER is extremely difficult and expensive. It is also assumed that the aim of the magnetic design and the underlying research and development should provide a design that is qualified for the generator lifetime.

The expected pulse length of ITER is several thousand seconds. During such a long time, the DC component of the magnetic field generated by the plasma is relatively large. This quasi-stationary component of the magnetic field has to be measured by a sensor that is sensitive directly to magnetic field, and not to its time derivative. It appears that the best candidate for such a steady state magnetic sensor that has to complement to the traditional induction coils is based on Hall effect. The main advantages of the Hall sensor are: small dimensions, simple principle of operation, linear dependence of the output signal on magnetic field in a broad field range, and insensitivity to mechanical vibrations.

The aims of the project were to asses the best materials for the preparation of Hall sensors prototypes and to perform experimental verification of their expected properties by thermal cycling and subjecting to neutron irradiation.

The most important HS parameter is the magnetic sensitivity. It has to be sufficiently high for ITER diagnostic. This means that the Hall voltage, U_H must be sufficiently high. Of the three factors that constitute following equation:

$$R_H = -\frac{r}{en}$$

where e is the electronic charge, n is the electron concentration, and r is the Hall factor $(r \cong 1)$, only the technological factor μ/n is material dependent. Because of that it is a subject of choice and unavoidable limitations. Once the Hall Sensor (HS) is chosen as that of the measurement type, the other two technological factors depend on the proportions of the HS plate only. Thus they can be optimized for any material without any limitations.

Hence, if the high magnetic sensitivity is desired only, the best semiconductor material is that having high electron/hole mobility μ and low electron/hole concentration n. Summarizing the last remarks, one can conclude that high carrier mobility always improves the HS parameters, whereas low carrier concentration increases the HS sensitivity, but it can meaningfully degrade other HS parameters. The values of n(T) and μ (T) at room temperature and their temperature dependences are defining the basic parameters of Hall sensors.

The group of semiconductor contains two important compounds, InSb and InAs having the highest electron mobility at room temperature and above. These two compounds are most frequently used for the preparation of HSs. The other members of the family are: GaSb, InP, GaP, GaN and AlN. Other physical properties of semiconductor materials, which are decisive for their use in the preparation of HSs for ITER are: the ability to work at elevated temperature and strong neutron irradiation.

In the present experimental studies we used high-temperature Hall sensors developed at Instytut Fizyki Politechnika Poznanska. An important part of these sensors is their high temperature casing. The sensors are suitable for working at temperatures up to 300° C. In our experiments we subjected both the HSs as whole and their constructional materials to neutron irradiations and to subsequent investigation of the irradiation effects. In addition to that we performed thermal cycling of the irradiated HSs, as a rule to 300° C, and investigated the effect of the annealing. We consider the thermal cycling as being a very important procedure because it may appear that it will have to be used to extend lifetime of the sensors in the ITER conditions. For the experimental studies eight (8) complete Hall sensors (HS) were prepared. Half of them will be constructed on the Al₂O₃ base plates and the second half will be constructed on the AlN base plates. For each base plate, half of the HS will be protected with the InSb/CdTe shields.

This investigation gives us the info if both the base plate materials are equivalent. It also gives an answer to the question, how much effective is the shield with reference to the HS. The HS are numbered and their parameters are given in the table below

Sample Nr:	Hall sensor parameters					
	d [µm]	R [Ω]	$\mu [cm^2/Vs]$	n [cm ⁻³]		
C-2	0,90	7,2	5560	4,38*10 ¹⁸		
C-3	0,90	20,6	7680	1,10*10 ¹⁸		
C-4	0,90	10,7	5790	2,80*10 ¹⁸		
C-6 *)	0,90	10,5	5760	2,87*10 ¹⁸		
C-7 *)	0,90	10,4	5700	2,94*10 ¹⁸		
C-8 *)	0,90	12,5	5040	2,76*10 ¹⁸		
C-9	0,90	9,9	5780	3,04*10 ¹⁸		
C-10 *)	0,90	10,2	5680	3,00*10 ¹⁸		

The HSs for the third irradiation are shown in Fig. 1



Fig.1.

Irradiation of Hall sensors, based on thin InSb layers and developed in Poznan Technical University, was performed in fission reactor LVR-15 in NRI in Řež. The sensors were exposed to neutron fluence of 1.12×10^{17} cm⁻² with fission-like neutron spectra. Part of the samples was shielded with CdTe/InSb glass in order to assess effect of transmutation on physical properties of the Hall sensors.

Input/output resistances, offset voltages, sensitivities, free charge carrier density, and charge mobility before and after the irradiation were measured. The radiation induced changes of parameters of the sensors are very small and comparable for shielded and unshielded sensors, so no apparent effect of the *CdTe/InS*b shielding was observed. Possibly, the occurred minor changes of sensors parameters are affected by elevated temperature during the irradiation rather than by the irradiation itself.

The main component of the sensors responsible for long term activation was found to be silver-based high temperature contacting paste. Clearly, application of another method for providing electrical contacts to the thin film e.g. ultrasonic bonding or thermo compression, would strongly reduce activation and consequently it would shorten the delay between irradiation and post-irradiation analysis even for higher total neutron fluences. Post-irradiation annealing of the sensors at 350°C for 20 minutes resulted in permanent increase of free charge carriers mobility and decrease of their density suggesting the partial annealing of the structural defects within the InSb semiconductor material. As a result, we conclude that

annealing is a perspective complementary method, besides optimized sensors doping and in-situ recalibration techniques, which can help to ensure stable performance of the Hall sensors in radiation environment. Measured changes of the free charge carrier density of the InSb sensing layers are similar to the value obtained from simulation of the transmutation of InSb sensing layer performed by FISPACT code which further motivates use of this code complementing further irradiation experiments. Future exposure of the sensors to neutron fluence of the order of 10^{18} cm⁻² is envisaged in order to obtain more pronounced radiation induced effects and consequently, to enable more quantitative conclusions to be drawn.

Studies of double passage of electromagnetic waves through magnetized plasma and other recent results in plasma diagnostics: diffraction problem, self-focusing and plasma tomography

In the year 2009, Maritime University of Szczecin, Poland, jointly with WPUT, studied methods in microwave and infrared plasma diagnostics, embracing the following five problems:

- 1) Double passage scheme in polarimetry and interferometry
- 2) Eligibility of localized plasma polarimetry, based on mode conversion in tokamaks.
- 3) Non-conventional procedure of polarimetry data inversion in conditions of comparable Faraday and Cotton-Mouton effects
- Revealing of Limited accuracy of the Cotton-Mouton polarimetry in the toroidal plasma with helical magnetic lines Besides, additional topic was studied,
- 5) Analysis of electromagnetic waves diffraction in plasma in presence of nonlinear phenomena, which relates to the problem of plasma heating by powerful microwave beams.

1. Double passage scheme in polarimetry and interferometry

Properties of electromagnetic waves, reflected from the target of a magnetized plasma, are studied above with a special emphasis on plasma polarimetry in thermonuclear reactors ITER and W-7X. An analysis is carried out for independent normal modes, propagating both in homogeneous and inhomogeneous media. Advantages and shortcomings of double passage regime in plasma polarimetry-interferometry system were analyzed. The main advantage is reduction of the amount of windows in tokamak camera. However, this positive effect is accompanied by influence of polarization state on interferometry channel. A few methods are considered which might reduce polarization dependence on interferometry channel, including following methods: transition to higher frequencies, using polarization transformation of the signal or the reference beam, automatic adjusting of polarization in the signal channel, implementation of a 2D corner reflector.

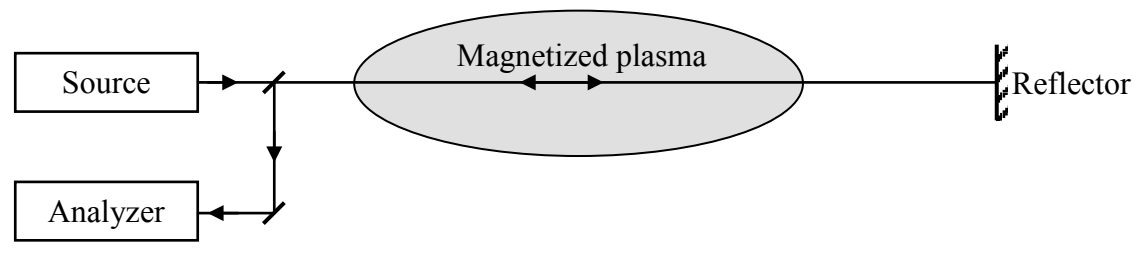


Fig. 1. Scheme for double-passage measurements

An electromagnetic wave, reflected from a metallic plane and from a CCR is shown to contain only "velocity-preserving" channels of scattering, when the fast (slow) normal wave also reproduces, after reflection, the fast (slow) normal wave. As a result, the phases of the reflected waves become doubled in comparison with the single-passage propagation. This fact, known earlier for the pure Faraday effect

(circularly polarized waves) and for the pure Cotton-Mouton effect (linearly polarized normal waves) is generalized now for elliptically polarized, non-interacting normal waves of the general type in the frame of quasi-isotropic approximation and is in concordance with analysis, based on Stokes vector and Mueller matrix formalism.

At the same time, the wave reflection from a 2D-corner retro-reflector (2D-CR) is characterized by the appearance of both "velocity-preserving" and "velocity-converting" channels, the latter transforming the fast wave into the slow one and vice-versa. It is shown that in the case of circularly polarized modes, the "velocity-preserving" channels completely disappear, and only "velocity-converting" channels exist. As shown above, for these channels, the initial polarization state of the electromagnetic wave is restored after double passage through magnetized plasma. This kind of the double passage scheme is of special interest for plasma interferometry.

2. Eligibility of localized plasma polarimetry, based on mode conversion in tokamaks

Phenomenon of linear modes conversion in the inhomogeneous plasma is widely known in electromagnetic theory. It was studied first in respect to solar corona and later in the Earth's ionosphere. Such a phenomenon, being applied to tokamak plasma, might form a basis for localized plasma polarimetry, using circular modes conversion in the vicinity of orthogonality point between the sounding beam and static magnet field.

Unfortunately, promising theoretical prerequisites have met strong practical limitations. Detailed analysis of the problem has shown that localized plasma polarimetry can be produced in tokamaks only in condition of super dense plasma with $N_e>10^{17} cm^{-3}$, what is 1000 times higher than the ITER project envisages.

3. Non-conventional procedure of polarimetry data inversion in conditions of comparable Faraday and Cotton-Mouton effects

New procedure for plasma polarimetry data inversion is suggested, which fits two parameter knowledge-based plasma model to the measured parameters (azimuthal and ellipticity angles) of the polarization ellipse. The knowledge-based model is supposed to use the magnetic field and electron density profiles, obtained from magnetic measurements and lidar data on the Thomson scattering. In distinction to traditional polarimetry, polarization evolution along the ray is determined from the equations for angular parameters of polarization ellipse. The method under consideration is applicable in conditions, when Faraday and Cotton-Mouton effects are simultaneously strong. The first results of numerical modelling illustrate ability of the new method to describe strong polarization changes of the wave, passed through magnetized plasma.

4. Revealing of limited accuracy of the Cotton-Mouton polarimetry in the toroidal plasma with helical magnetic lines

Cotton-Mouton effect in the sheared plasma with helical magnetic lines is studied on the basis of the equation for complex amplitude ratio (CAR). A simple model for helical magnetic lines in plasma of toroidal configuration is suggested. An equation for CAR is solved by perturbation method, using smallness of the shear angle variations, caused by the spiral form of magnetic lines. It is shown that inaccuracy of polarization measurements in toroidal plasma with the spiral form of magnetic lines does not exceed 1.0-2.0 %, what determines the limit accuracy of Cotton-Mouton polarimetry. The method of preliminary subtracting of the "sheared" term is suggested, which may significantly improve an accuracy of Cotton-Mouton polarimetry.

6. Self-focusing in nonlinear plasma

Important result was obtained in wave diffraction in presence of nonlinearity. It is shown that nonlinear processes like self-focusing can be described in the frame of the complex geometrical optics, which deals with ordinary differential equations and significantly simplified analysis of non-linear phenomena.

Complex geometrical optics (CGO), dealing with the Gaussian beams, was generalized in the year 2009 [Berczynski, Kravtsov, Sukhorukov] for the case of nonlinear media. It was shown that CGO effectively describes behavior of Gaussian beam in nonlinear media, including phenomenon of self-focusing. The great advantage of CGO is in the fact, that it describes nonlinear diffraction processes in the frame of ordinary differential equations. This method looks quite prospective for analysis of nonlinear phenomena, arising under microwave heating in tokamaks. Recent studies have shown that the method under development allows studying influence of the initial curvature of the phase front of the incident power beam. The CGO results were compared with the FD-BPM method of quasi-optical family, which operates with equations in partial derivatives and frequently is used in optics for description of diffraction phenomena. It was shown that accuracy of complex geometrical optics is comparable with rigorous diffraction methods. In the same time CGO demonstrates 50-times higher rate of calculation as compared with FD-BPM.

The CGO results were compared with the FD-BPM method of quasi-optical family, which operates with equations in partial derivatives and frequently is used in optics for description of diffraction phenomena. It was shown that eikonal-based CGO demonstrates 50-times higher rate of calculation as compared with FD-BPM.

The method, which is under consideration looks quite prospective for analysis of nonlinear phenomena, arising under microwave heating of plasma.

	Physics and Technology of Fusion
Inertial fusion energ	gy "keep-in-touch" activity

Coordinated study of phenomena related to impact fast ignition of ICF targets. Investigation of properties of the plasma jet generated from materials with various atomic number for ICF applications

The investigations carried out on the PALS concerns two problems, namely:

- A. Experimental and theoretical investigations of mechanisms responsible for plasma jets formation
- **B.** Developing the new indirect method for two-step acceleration of the thin foil to high velocity-RAS Reverse Acceleration Scheme

Regarding the first one, the experiments (A) were carried out with the use of the PALS iodine laser facility. Plasma was generated by a laser beam of the diameter about 160 mm, which was focused by means of an aspherical lens with focal lengths of 600 mm for the third harmonic used (λ =0.438 μ m). The plastic and Cu planar targets were irradiated by the laser beam under the following conditions: laser energy of 30 J, focal spot radius of 400 μ m (whereas the focal point was located inside the targets), and the pulse duration of 250 ps (FWHM). In this case the average laser intensity is $0.24 \cdot 10^{14} \, \text{W/cm}^2$.

To study plasma expansion a 3-frame interferometric system was used. To register the X-ray plasma radiation changes in the vicinity of the target surface the X-ray streak camera was applied.

The interferometric measurements corresponding to the high-Z (Cu) and low-Z (plastic) target materials are presented in Fig. 1.

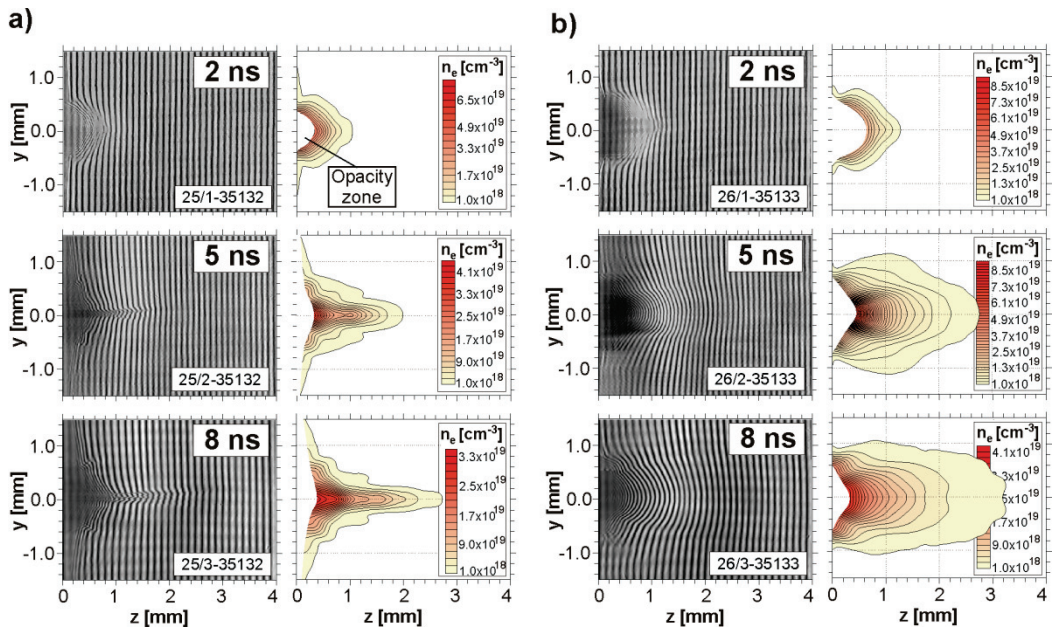


Fig. 1. Sequences of interferograms and electron equidensitograms showing evolution of plasma structure. in the case of: a) Cu and b) plastic target

In both cases plasmas have tendency towards plasma jet creation. The great difference in the plasma outflow structure appears on the second frame (Δt =5 ns). In the case of Cu target a jet creation process is continued, whereas the plastic plasma expansion changes essentially and assumes a divergent character. Instead, measurements of the plasma radiation by the streak camera shows that for both targets the annular form of the X-ray radiation seems to be dominant. However, in the case of the plastic target at a certain instant of the laser action additional radiation in the center appears. An attempt of explanation of it was taken by means of numerical simulations of the laser beam interactions with the planar Cu and plastic targets using the two-dimensional hydrodynamic code ATLANT-HE. The computations were performed for the PALS radiation conditions. A homogeneous target irradiation was assumed. The calculations were performed using the equation of the perfect gas. The most important achievement of these simulations was finding the additional mechanism that takes part in the plasma jet forming toward the two such mechanisms considered so far, namely the annular irradiation and the plasma radiative cooling. Based on numerical simulations, the influence of the plasma expansion regime was identified: in

the case of Cu, the *planar* expansion regime is taking place and in the case of plastic, it is the *spherical* one. In our opinion, all these three mechanisms play their respective roles in the plasma jet forming. The obtained scientific material, both experimental and theoretical, is inspiring for formulating of new ideas, concerning both improvements of the plasma stream parameters and the creation of more composite configurations of plasma jet, useful to plasma researches, connected with the realization of ICF.

In the case of the second studies (**B**) the following laser parameters for targets irradiation have been chosen: the first harmonic of laser radiation (λ =1.315 µm) with an energy in the range of 120-500 J, a pulse duration of 250 ps (FWHM) and focal spot diameters at the target surface 100 – 200 µm. The "cavity type" targets consisted of a massive Al slab with a cylindrical hole of 600 µm in diameter and 100 µm in depth as well as 10, 300 or 500 µm thick Al foils covering a hole. So, the targets constituted a closed cavity, Fig. 2.

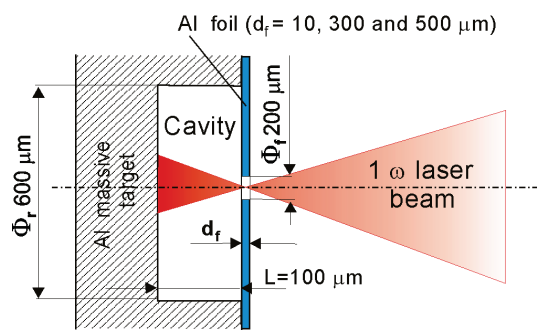


Fig. 2. Construction of the "cavity type" targets used in the experiment.

To study the flayer foils dynamics and deformation a three-frame shadographic/interferometric system was employed. Investigations of the 10 μ m thick Al foil acceleration were carried out for the three laser energies mentioned above. The foil reached velocities in the range of (2-3)·10⁷ cm/s. The velocities of the 300 μ m thick foil for the laser energies of 120, 300 and 500 J were determined to be equal to $0.7 \cdot 10^7$ cm/s, $1.0 \cdot 10^7$ cm/s and $1.4 \cdot 10^7$ cm/s, respectively.

The obtained results demonstrate that the proposed scheme can be applied to accelerate macroparticles to high velocities with efficiency not observed in classic ablative experiments. These results clearly show that the most important element of the applied method of acceleration is pressure produced in the target cavity. So, this mechanism can be named as a "Cavity Pressure Acceleration Scheme" (CPAS). Our results (high velocity of accelerated foil/macroparticle or possibility of accelerating heavy macroparticles) show that they can be applied to study impact fast ignition and impact fusion problems. This method leads to significantly higher velocities of flyer foils than those obtained by traditional way (ablative acceleration scheme) in similar experimental conditions. It follows from the fact that CPAS allows to use almost all absorbed laser energy (neglecting the energy of the shock wave propagating into the solid target). Also the hydrodynamic efficiency of the energy transfer to the flyer foil is much higher. CPAS enables acceleration by laser of very heavy macroparticles ($\rho d_f \sim 10^{-1} \text{ g/cm}^2$) to velocities of $\sim 1\cdot10^7$ cm/s (authors do not know similar results in the literature) whereas conventional ablative acceleration of that foil was completely unsuccessful (the foil has even not started).

Р	hysics	and	Techr	nology	of of	Fusion
So	cio-	Eco	nom	ic Re	ese	arch

Building the methodology to investigate the effects of two selected communication strategies (approaches,s methods) on fusion understanding among selected publics/stakeholders

In the year 2009, the work has been focused on defining the core concepts of the research and their operationalization. Finally, it was decided that the dependent variable is labeled "understanding fusion as an energy option" and set up as a two-dimensional construct of an attitude being a combination of two components: cognitive and emotional/axiological. The first consists in awareness of fusion and knowledge of it as an energy option, and has to be measured on sub-dimensions: technological/scientific and economic/environmental. The second – consisting in feelings about fusion as an energy option - has to be measured on up to four sub-dimensions: (i) subjective risk assessment in relation to fusion, the level of fear of it; (ii) level of cognitive interest in fusion as an energy source; (iii) general evaluation of fusion, level of its acceptance; and (iv) disposition to support fusion as an energy option within public debate, to vote for it.

The independent variable has been labeled as "strategy of communication on fusion" and denotes communicated content in two variants: describing fusion with focus on (a) technological and scientific aspects and on the other hand (b) on economic and environmental aspects.

Quantitative analysis of dependence of the dependent variable "understanding fusion as an energy option" on the independent one, "strategy of communication on fusion", will be conducted with control of a respondent's major. Values of respective controlling variable are the following majors: (1) sociology / political sciences / journalism; (2) economic sciences / economics; (3) physics and (4) ecology and environment.

The main achievements are as follows:

- 1. The list of criteria necessary to score the level of knowledge on fusion as an energy option has been set up;
- 2. The test of knowledge on fusion as an energy option has been prepared to be applied in the main stage of the research (individual questionnaires).